REPORT DOCUMENTATION PAGE

Form Approved OMB NO. 0704-0188

1. REPORT DATE (DD-MM-YYYY)	2. REPORT TYPE	3. DATES COVERED (From - To)
13-03-2019	Final Report	1-Oct-2016 - 30-Sep-2018

4. TITLE AND SUBTITLE
Final Report: Research Area 9 Materials Science: Anistropic Microstructurally-engineered Polycrystals for increased Laser Engergy (AMPLE)

5a. CONTRACT NUMBER
W911NF-16-1-0571

5b. GRANT NUMBER

5c. PROGRAM ELEMENT NUMBER

6. AUTHORS

5d. PROJECT NUMBER

5e. TASK NUMBER

5f. WORK UNIT NUMBER

7. PERFORMING ORGANIZATION NAMES AND ADDRESSES
University of California - San Diego
Office of Contract & Grant Adm
9500 Gilman drive, MC 0934
La Jolla, CA 92093 -0934

8. PERFORMING ORGANIZATION REPORT NUMBER

9. SPONSORING/MONITORING AGENCY NAME(S) AND ADDRESS (ES)
U.S. Army Research Office
P.O. Box 12211
Research Triangle Park, NC 27709-2211

10. SPONSOR/MONITOR'S ACRONYM(S)
ARO

11. SPONSOR/MONITOR'S REPORT NUMBER(S)
69658-MS.1

12. DISTRIBUTION AVAILIBILITY STATEMENT
Approved for public release; distribution is unlimited.

13. SUPPLEMENTARY NOTES
The views, opinions and/or findings contained in this report are those of the author(s) and should not contrued as an official Department of the Army position, policy or decision, unless so designated by other documentation.

14. ABSTRACT

15. SUBJECT TERMS

16. SECURITY CLASSIFICATION OF:			17. LIMITATION OF ABSTRACT	15. NUMBER OF PAGES	19a. NAME OF RESPONSIBLE PERSON
a. REPORT	b. ABSTRACT	c. THIS PAGE			Javier Garay
UU	UU	UU	UU		19b. TELEPHONE NUMBER 858-534-0280

RPPR Final Report
as of 03-Apr-2019

Agency Code:

Proposal Number: 69658MS **Agreement Number: W911NF-16-1-0571**
INVESTIGATOR(S):

Name: Javier Garay jegaray@en
Email: jegaray@ucsd.edu
Phone Number: 8585340280
Principal: Y

Organization: **University of California - San Diego**
Address: Office of Contract & Grant Adm, La Jolla, CA 920930934
Country: USA
DUNS Number: 804355790 EIN: 956006144
Report Date: 31-Dec-2018 Date Received: 13-Mar-2019
Final Report for Period Beginning 01-Oct-2016 and Ending 30-Sep-2018
Title: Research Area 9 Materials Science: Anistropic Microstructurally-engineered Polycrystals for increased Laser Engergy (AMPLE)
Begin Performance Period: 01-Oct-2016 **End Performance Period:** 30-Sep-2018
Report Term: 0-Other
Submitted By: Javier Garay Email: jegaray@ucsd.edu
Phone: (858) 534-0280
Distribution Statement: 1-Approved for public release; distribution is unlimited.

STEM Degrees: 3 **STEM Participants:** 5

Major Goals: The overall goal of this project is to replace the typical cubic oxides traditionally used as gain media with a much higher conductivity rare earth (RE) doped aluminum nitride (AlN), i.e. to develop RE:doped aluminum nitride ceramics as viable lasing media. Our approach is to consolidate nitride powder to full density without significantly increasing the grain size using current activated pressure assisted densification CAPAD.
In this project we made significant progress toward our goals. We have now successfully doped Tb, Nd, Eb and Tm into Al2O3 and AlN and demonstrated emission over the entire range of 1 to 2 ?m. We showed very high thermal conductivities >90 W/m.K (compared to ~10 W/m.K for the state of the art). Perhaps the most noteworthy accomplishment was demonstrating and quantifying optical gain in our ceramics (in Nd:Al2O3), proving that they are viable laser ceramics. This achievement represents a new paradigm of laser ceramics and unambiguously shows that ceramics non-cubic crystal structures can be used for gain media. These materials are promising gain materials for high average power lasers. This achievement received significant worldwide media attention (Optics.org, Photonics.com, Materials Today, etc.)

Accomplishments: In this project we made significant progress toward our goals. We have now successfully doped Tb, Nd, Eb and Tm into Al2O3 and AlN and demonstrated emission over the entire range of 1 to 2 ?m. We showed very high thermal conductivities >90 W/m.K (compared to ~10 W/m.K for the state of the art). Perhaps the most noteworthy accomplishment was demonstrating and quantifying optical gain in our ceramics (in Nd:Al2O3), proving that they are viable laser ceramics. This achievement represents a new paradigm of laser ceramics and unambiguously shows that ceramics non-cubic crystal structures can be used for gain media. These materials are promising gain materials for high average power lasers. This achievement received significant worldwide media attention (Optics.org, Photonics.com, Materials Today, etc.)

Training Opportunities: PhD students worked on this project and graduated primarily supported by this project. They are:
Andrew Weig PhD, 2015
Elias Penilla PhD 2016
Matthew Duarte PhD, Expected 2019

RPPR Final Report
as of 03-Apr-2019

Results Dissemination: The PI gave many invited presnetations based on results of this projeytc. Some of Thhese include:
(Invited Speaker) Processing and properties of transparent anisotropic ceramics Electronic Materials and Applications Conference, Orlando, Florida, Jan 2017
(Invited Speaker) "Microstructure-processing-property Relationships in Nanocrystalline Ceramics Produced Using Current-activated, Pressure-assisted Densification (CAPAD)" 2017 TMS Annual Meeting & Exhibition. 02/28/2017
(Invited Speaker) “Microstructure/property Relationships for Light Transmission, Absorption and Emission in Optical Ceramics” MS&T 16, Salt Lake City, Utah 24–26 October 2016

The results were disseminated in top peer reviewed archival materials science, applied physics and optics journals:

E. H. Penilla, Y. Kodera and J. E. Garay, “Blue-green emission in terbium doped alumina (Tb: Al2O3) transparent ceramics” Advanced Functional Materials (2013) 23, 6036–6043

A. T. Wieg, Y. Kodera, Z. Wang, C. Dames and J. E. Garay
“Thermo-mechanical properties of rare earth doped AlN for laser applications: The role of grain boundaries and grain size” Acta Materialia (2015) 86, 148-156.
V. Mishra, C. L. Hardin, J. E. Garay and C. Dames, "A 3 omega method to measure an arbitrary anisotropic thermal conductivity tensor", Rev. of Sci. Instruments 86 (2015) 054902

T. Hori, J. Shiomi, C. Dames, “Effective phonon mean free path in polycrystalline nanostructures.” Applied Physics letters (2015) 106, 171901

A. T. Wieg, Y. Kodera, Z. Wang, C. Dames and J. E. Garay, “Thermomechanical properties of rare earth doped AlN for laser gain media: The role of grain boundaries and grain size” Acta Materialia (2015) 86, 148-156.

E. H. Penilla, C. L. Hardin, Y. Kodera, S. A. Basun, D. R. Evans and J. E. Garay, “The role of scattering and absorption on the optical properties of birefringent polycrystalline ceramics: Modeling and experiments on ruby (Cr: Al2O3)” Journal of Applied Physics (2016) 119, 023106

A. T. Wieg, M. J. Grossnickle, Y. Kodera, N. M. Gabor and J. E. Garay, “Nd:AlN polycrystalline ceramics: A candidate media for tunable, high energy, near IR lasers” Applied Physics Letters 109, 121901 (2016)

A. T. Wieg, E. H. Penilla, C. R. Hardin, Y. Kodera and J. E. Garay, “Broadband white light emission from Ce:AlN ceramics: High thermal conductivity down-converters for LED and laser-driven solid state lighting” APL Materials, 4, 126105 (2016); doi: 10.1063/1.4971846 (2016)

E. H. Penilla, L. Devilla, M. Duarte C. Hardin, Y. Kodera, and J. E. Garay, “Gain in Nd doped alumina Transparent ceramics for high energy laser applications”, Light: Science & Applications. (2018) 7, doi:10.1038/s41377-018-0023-z

F. Kargar, E. H. Penilla, E. Aytan, J. S. Lewis, J. E. Garay and A. A. Balandin “Acoustic Phonon Spectrum Engineering in Bulk Crystals via Incorporation of Dopant Atoms” Applied Physics Letters. 112, 191902 (2018); doi: 10.1063/1.5030558

M. Duarte a, V. Mishra b, C. Dames b, Y. Kodera a and J. E. Garay, “Processing and thermal conductivity of bulk nanocrystalline aluminum nitride.” In review (2019).

Honors and Awards: Nothing to Report

Protocol Activity Status:

Technology Transfer: This work led to the submission of one Provisional Patent application:
RARE-EARTH-DOPED ALIMUNA-OXIDE LASER GAIN MEDIA
Application #:62797139
1/25/2019

RPPR Final Report
as of 03-Apr-2019

PARTICIPANTS:

Participant Type: Faculty
Participant: Javier E Garay
Person Months Worked: 6.00 **Funding Support:**
Project Contribution:
International Collaboration:
International Travel:
National Academy Member: N
Other Collaborators:

Participant Type: Faculty
Participant: Yasuhiro Kodera
Person Months Worked: 6.00 **Funding Support:**
Project Contribution:
International Collaboration:
International Travel:
National Academy Member: N
Other Collaborators:

Anisotropic Microstructurally-engineered Polycrystals for increased Laser Energy (AMPLE)
PI.: J. E. Garay, UC San Diego (FINAL reoprt 2019)

Abstract (Not to exceed 200 words)
The overall goal of this project is to replace the typical cubic oxides traditionally used as gain media with a much higher conductivity rare earth (RE) doped aluminum nitride (AlN), i.e. to develop RE:doped aluminum nitride ceramics as viable lasing media. Our approach is to consolidate nitride powder to full density without significantly increasing the grain size using current activated pressure assisted densification CAPAD.
In this project we made significant progress toward our goals. We have now successfully doped Tb, Nd, Eb and Tm into Al2O3 and AlN and demonstrated emission over the entire range of 1 to 2 μm. We showed very high thermal conductivities >90 W/m.K (compared to ~10 W/m.K for the state of the art). Perhaps the most noteworthy accomplishment was demonstrating and quantifying optical gain in our ceramics (in Nd:Al_2O_3), proving that they are viable laser ceramics. This achievement represents a new paradigm of laser ceramics and unambiguously shows that ceramics non-cubic crystal structures can be used for gain media. These materials are promising gain materials for high average power lasers. This achievement received significant worldwide media attention (Optics.org, Photonics.com, Materials Today, etc.)

Example of Rare earth doped samples by reactive processing in CAPAD

a) Nd: doped Aluminum Nitride

Luminescence from rare earth (RE) dopants is important for a wide range of optoelectronic devices such as optical amplifiers and solid-state lasers. Perhaps the most common RE ion in optical gain media is Nd, in part because of its high absorption cross section. Since they were first demonstrated, [1] Nd:YAG single crystals have been the mainstay material for solid-state lasing media. High quality Nd-doped glass (Nd:Glass) is also pervasive, since there are strong advantages to both glasses and crystalline hosts. Nd:YAG has sharper emission lines, leading to lower lasing thresholds compared to Nd:Glass. However, the broader lines in glass hosts can be advantageous since they can lead to amplification of shorter temporal pulses. Broadened lines can also deliver high energy; In fact, some of the highest energy lasers are based on Nd:Glass [2]. One of the main detractors to glass as a gain media is the low thermal conductivity, k (~ 1 W/m·K *vs.* 10 to 14 W/m·K for Nd:YAG) because deliverable power scales with k. Nd:YAG is used in continuous wave (CW), or high repetition rate applications since it exhibits narrow line widths and high thermal conductivity. Nd:Glass, on the other hand, is the better choice for high pulse energy, low repetition rate applications. Here, we report on a Nd:AlN ceramic which displays traits of both single crystal and glass hosts.

The very high k of AlN (up to 300 W/m·K [3]) has generated widespread interest for a variety of photonic applications. Production of RE:AlN has steep processing challenges including susceptibility to oxygen contamination, degrading k, birefringence, decreasing transparency and low dopant solubility, limiting effective light emission. Despite the challenges, significant work has been devoted to RE:AlN thin films [4,5] and powders [6] for light emission applications. Ceramics have also gained importance as laser gain media [7], prompting studies of RE:AlN ceramics for solid-state laser gain media [8-10]. Merkle *et al.* demonstrated successful incorporation of Er into translucent AlN leading to photoluminescence (PL) at ~1500 nm [8]. In previous work, [9] we showed PL in the visible from translucent Tb:AlN ceramics with a measured k = 94 W/m·K at room temperature (a 7 fold improvement on RE:YAG). Moreover, the Tb:AlN ceramics have superior mechanical properties in addition to higher k, leading to a thermal shock figure of merit increase of >60 times over RE:YAG [10].

Polycrystalline samples were processed from commercial AlN (97% purity as AlN, 1–2 μm particle size, Tokuyama, Japan) and Nd metal (99.9% purity, 200 mesh, Alfa Aesar) powders. Nd was added as NdN to produce AlN with 0.5 atomic % Nd. The metal Nd powder was loaded into the furnace tube in an Ar glovebox, before being transferred to the furnace. The Nd was then heated to 600 °C under flowing nitrogen for 6 h. The powders were mixed using planetary ball milling. Powders and silicon nitride milling media were loaded into silicon nitride jars and sealed under an argon atmosphere. Silicon nitride has been shown to produce less

contamination compared to other media [11]. A 10:1 ball:powder mass ratio was used and milling was performed at 450 rpm (Sample 1) or 600 rpm (Sample 2) for 3 h. Powders were collected under argon post milling.

Powders for CAPAD (current activated pressure assisted densification) [12, 13] were loaded into a graphite die (19 mm inner diameter) and plunger assembly under an argon atmosphere and processed using a custom built CAPAD apparatus. Samples were processed at 1700 °C (Sample 1) or 1750 °C (Sample 2) using 105 MPa and a heating rate of ~500 °C min^{-1}, in vacuum (~ 3×10^{-2} Torr). Temperature was measured using an optical pyrometer focused on the die wall.

Prior to characterization, samples were polished using diamond abrasive wheels followed by alumina paste on felt wheels to 0.5 μm. Microstructure was characterized using Philips FEG30 scanning electron microscope (SEM) with both secondary electron (SE) and backscatter electron (BSE) detectors. Grain size was measured by averaging >100 grains in SEM micrographs. X-ray diffraction with Cu-K_α radiation was conducted using a Panalytical Empyrean. Relative density was measured using the Archimedes method and theoretical density of AlN (3.26 g/cm^3).

Bulk PL of Nd;ALN was measured on a Horiba Jobin Yvon Fluorolog using an 808 nm laser diode as an excitation source. Laser quality single crystal 1.4 At% Nd:YAG doped and laser quality Nd:Glass were measured for comparison. SEM micrographs and 2D luminescence maps of the same areas of Nd:AlN were collected. Vickers indentation patterns were used as area markers. Spatially resolved PL was measured with a custom-built scanning microscope using a 500 fs pulsed-beam from a tunable Ti-Sapphire laser. Spatial PL maps were produced by raster scanning the diffraction-limited (FWHM = 500 nm) beam over the surface of the sample and measuring the emitted light using a single-pixel InGaAs photodetector. Measurements were conducted at 72 K and at room temperature (300 K).

Figure 1 shows SEM micrographs for samples produced using the two different processing procedures described above (**Fig. 1a** and **1b,** Sample 1) and (**Fig. 1d** and **1e,** Sample 2). Nd is significantly heavier than Al and N causing Nd-rich areas to appear brighter in micrographs (especially in BSE). The micrographs reveal that Sample 1 has significant dopant segregation along the grain boundaries and triple points while Sample 2 displays minimal dopant segregation. This degree of spatial dopant homogeneity is remarkable given that the ionic radius of Al^{3+} (0.57 Å) is small relative to the RE dopants. Demonstration of homogenous doping in AlN is rare; most previous studies on thin films [4,5] and ceramics [8] do not provide micrographs for assessing spatial homogeneity. The present work is an improvement over previously demonstrated spatial homogeneity of Tb dopant [9], considering that the ionic radius of Nd^{3+} (1.15 Å) is larger than Tb^{3+} (1.09 Å).

Samples 1 and 2 have an average grain size of 3.8 μm and 4.9 μm respectively. It is well known that porosity plays a major role in light transmission [7]. CAPAD processing yielded translucent Nd:AlN with >99% relative density in both samples. We previously showed that *k* is largely controlled by grain size in Tb:AlN [10]. Since the Nd:AlN produced in this work has the same dopant concentration and similar grain size, as the Tb:AlN we produced previously we expect similarly high thermal conductivity >90 W/m·K.

The influence of dopant segregation on the uniformity of luminescence can be determined by performing optical luminescence microscopy on the same locations as the SEM. 2D luminescence maps are shown in **Figure 1c** (Sample 1) and **1f** (Sample 2). Comparison reveals that PL is significantly more uniform in the sample with minimal dopant segregation. Careful observation shows that the brighter or darker regions do not correlate with the segregation *i.e.* the Nd-rich grain boundaries cannot be discerned in the PL maps. This can be explained by considering the significantly different wavelengths and penetration depth (activation volume) of electrons and photons. The penetration depth of the electrons is estimated to be ~1 μm while the photons can activate the entire thickness (1 mm) of the translucent samples. The lack of uniformity of the PL is due to differences in regional Nd concentration. It is likely that PL is quenched at agglomerated regions where the Nd concentration is high and energy is transferred through cross relaxation in neighboring Nd ions rather than photon emission.

Spatially homogeneous PL, such as that observed in our homogeneously doped Nd:AlN, is a key requisite for most photonic applications. We therefore focus on sample 2 and, in the following, present detailed spectroscopy using continuous wave (CW at λ = 808 nm) and pulsed excitation (λ = 700 -1000 nm). **Figure 2a** shows the luminescence spectrum for 0.5 Nd:AlN (sample 2) under CW 808 nm (diode laser) excitation at room temperature. The inset shows a picture of the translucent ceramic. The spectrum shows two groups of relatively

well-defined peaks in the vicinity of 1080 nm and 1350 nm. Similarly, **Figure 2b** shows PL spectra for Nd-doped commercial host materials; Nd:Glass and single crystal Nd:YAG both showing the 2 groups of lines near 1070 and 1350 nm that have been consistently attributed to $^4F_{3/2} \rightarrow {}^4I_{11/2}$ and $^4F_{3/2} \rightarrow {}^4I_{13/2}$ electronic transitions of Nd. The Nd:YAG shows multiple sharp well-defined lines while the Nd:Glass displays only two inhomogeneously broadened lines. This is expected since the number as well as width of luminescent lines depends on the host symmetry and inhomogeneous broadening can be attributed to the amorphous structure of glass.

When compared to Nd:YAG and Nd:Glass, our homogeneously doped Nd:AlN exhibits more, better-defined lines than in Nd:Glass but fewer, broader lines compared to single crystal Nd:YAG. In addition, comparison reveals a shift in the location of the maximum intensity peak for all 3 Nd host materials.

To directly compare the peak shapes and positions, we plot the spectrum for Nd:AlN along with the Nd:YAG red shifted by 9 nm and Nd:Glass red shifted by 20 nm in **Figure 2c**. Emission from Nd:AlN is significantly broader, forming an 'envelope' around both the glass and the single crystal emission lines. In order to determine if the Nd:AlN lines are homogeneously or inhomogeneously broadened, we fit our measured spectrum using Lorentzian and Gaussian line profiles (Gaussian shown in **Figure 2d).** The fits are both excellent; the Lorentzian profiles yielded an $R^2 = 0.9937$ and Gaussian $R^2 = 0.9954$. Thus it is not possible to unambiguously determine if the lines are thermally (homogenously) broadened or due to multiple locations of Nd, leading to inhomogeneous broadening. We believe however that the latter is more likely as will be discussed below.

We also measured PL resulting from tunable laser pulses. **Figure 3** shows luminescence excitation-emission maps at 72 K and 300 K. These are normalized by the maximum emission peak over the region of interest: excitation at 725 – 900 nm (1.71 – 1.38 eV) and emission at 1000 to 1400 nm (1.24 – 0.89 eV) covering the $^4F_{3/2} \rightarrow {}^4I_{11/2}$ and $^4F_{3/2} \rightarrow {}^4I_{13/2}$ transitions. At 72 K, the most intense emission is due to the $^4F_{3/2} \rightarrow {}^4I_{11/2}$ transition (with a maximum at 1077 nm) while exciting between 730-750 nm. Excitation at ~800 nm causes the second brightest emission from the same transition. Two more excitation regions (~825 and ~860 nm) cause emission in the same region at lower excitation energies.

The 300 K luminescence maps show the brightest emission in four similar regions to those observed at 72 K. The greatest difference is the broader emission bandwidth. Another difference is that the three lower energy excitation bands are wider and are accessible at lower excitation energies (down to 875 nm). The emission at 1105 nm has increased to the point that it rivals the intensity of the 1077 line observed at higher energy excitation (~ 750 and ~ 800 nm). These differences are likely due to the thermal population of additional emitting levels at 300 K.

The effect of excitation wavelength on emission can be seen in PL maps in **Figure 4**. These are similar to those in **Figure 3**, but are normalized to the maximum intensity of each excitation wavelength instead of global intensity. Brighter colors signify more intense emission for a given excitation wavelength. At 72K, the 1077 line is the dominant for almost all excitation wavelengths. However, in the region ~825 to ~840 nm the line at 1105 nm rivals the 1077 emission as observed previously in **Figure 3**.

As mentioned earlier, it is likely that observed line broadening under laser excitation is caused by Nd situated on multiple locations within the Nd:AlN microstructure. AlN has the Wurtzite structure and presumably, Nd^{3+} would dope onto the Al^{3+} sites. The Al sites are all equivalent (Al sites are surrounded by four nitrogen atoms forming a distorted tetrahedron), thus Nd substituted on Al sites should be indistinguishable barring other defects. However, if Nd-dopants are associated with vacancies or interstitials distinguishable sites arise. Previous work by Metcalfe *et al.* identified one dominant Nd site and two minority sites in epitaxial Nd:AlN films [14]. They also observed broad emission (< 50 nm) at room temperature although the emission was red shifted compared to the present work. Epitaxial films often have emission shifts compared to bulk crystals caused by lattice strain. Multiple RE sites were also observed in previous work on AlN Er-doped ceramics [8]. Nd associated with grain boundary regions in polycrystalline ceramics are also likely alternative sites. Thus we believe that Nd located at multiple sites is the dominant source of line broadening.

We also consider the uniaxial structure of AlN, which may contribute to linewidth broadening. AlN has hexagonal symmetry leading to anisotropy in both absorption and emission. In our polycrystalline samples, the PL is likely the spatially-averaged emission of individual randomly oriented grains. Such anisotropic effects have been observed previously in other non-cubic Nd hosts [15-17].

Although broad emission leading to high tunability ranges are typically transition metal based (e.g., Ti:sapphire), successful RE-based tunable lasers exist. Stoneman and Esterowitz demonstrated continuously tunable lasers based on Tm:YAG and Tm:YSGG [18]. The emission spectra of Tm:YAG shows overlapping lines resulting in laser tunability from 1870 to 2160 nm [18]. It is possible that the overlapping lines we observe (**Figure 2**) could lead to similar tunability in the 1050 to 1150 nm range. The excitation-emission map of **Figure 4** reveals that one can tune the location of brightest intensity by carefully choosing the excitation wavelength, and at 300 K, the dominant line is more sensitive to excitation wavelength. It may be possible to exploit this feature, producing a laser tunable in this relatively large range. Finally, we note the possibility that Nd:AlN could potentially produce lasing at two wavelengths (so-called bichromatic lasing) similar to Nd-doped fluoride glasses [19]

In summary, we investigated the spatial distribution of PL for samples produced using different procedures. The sample with uniform dopant distribution resulted in significantly more uniform PL distribution. Nd:AlN ceramics showed significantly broader PL bandwidth than Nd:YAG and Nd:Glass. The results demonstrate that Nd:AlN holds potential for tunability over a broad range. In addition, there is opportunity for emission tunability by controlling excitation wavelength.

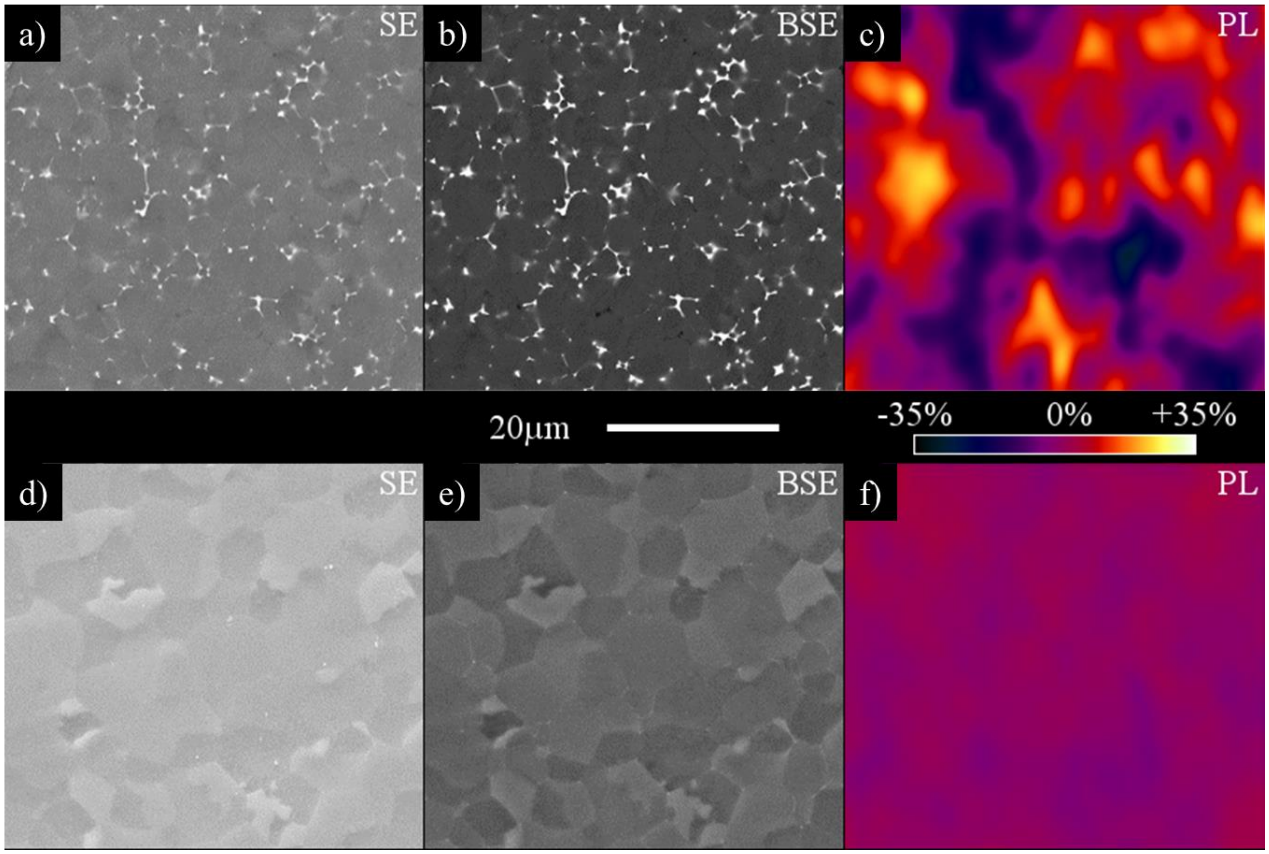

Figure 1: SEM (SE and BSE) micrographs and photoluminescence maps for Nd:AlN taken at the same location for Sample 1 (a, b, c) and Sample 2 (d, e, f). The SEM reveals significantly less dopant segregation in Sample 2 compared to Sample 1. The luminescence maps were taken using narrow band excitation at 808 nm and monitoring at 1064 nm.

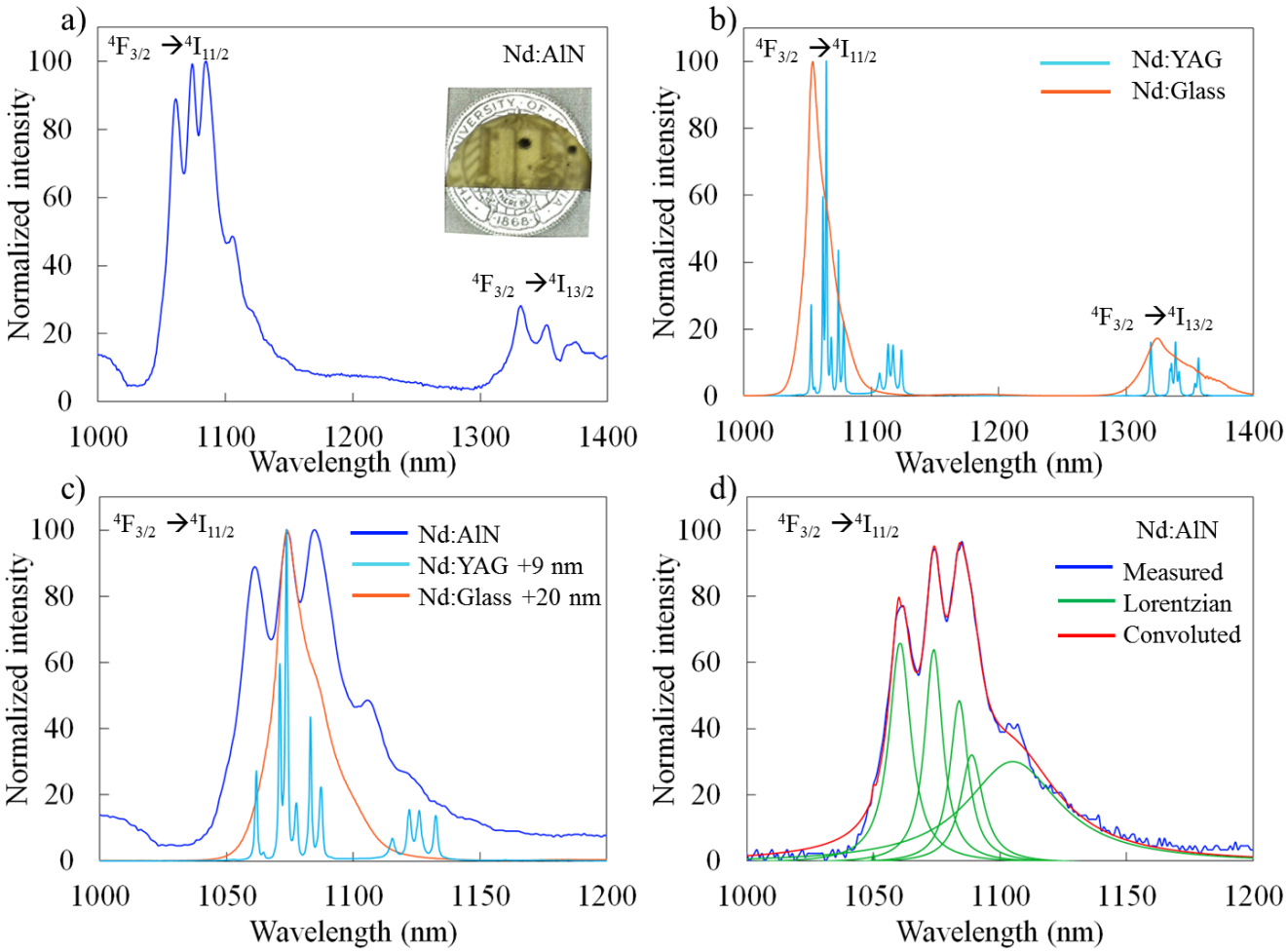

Figure 2. Luminescence spectra for various samples taken with 808 nm diode excitation at room temperature (a) 0.5 at% Nd:AlN. Inset: Picture of Nd:AlN sample (b) Emission spectra for commercially available Nd:Glass and single crystal Nd:YAG (c) 0.5 at% Nd:AlN (Sample 2) plotted together with commercially available Nd:YAG and Nd:Glass whose spectra have been red shifted by 9 nm and 20 nm respectively. (d) Gaussian deconvolution of 0.5 at% Nd:AlN spectra showing homogeneous broadening characteristic of inhomogeneous broadening.

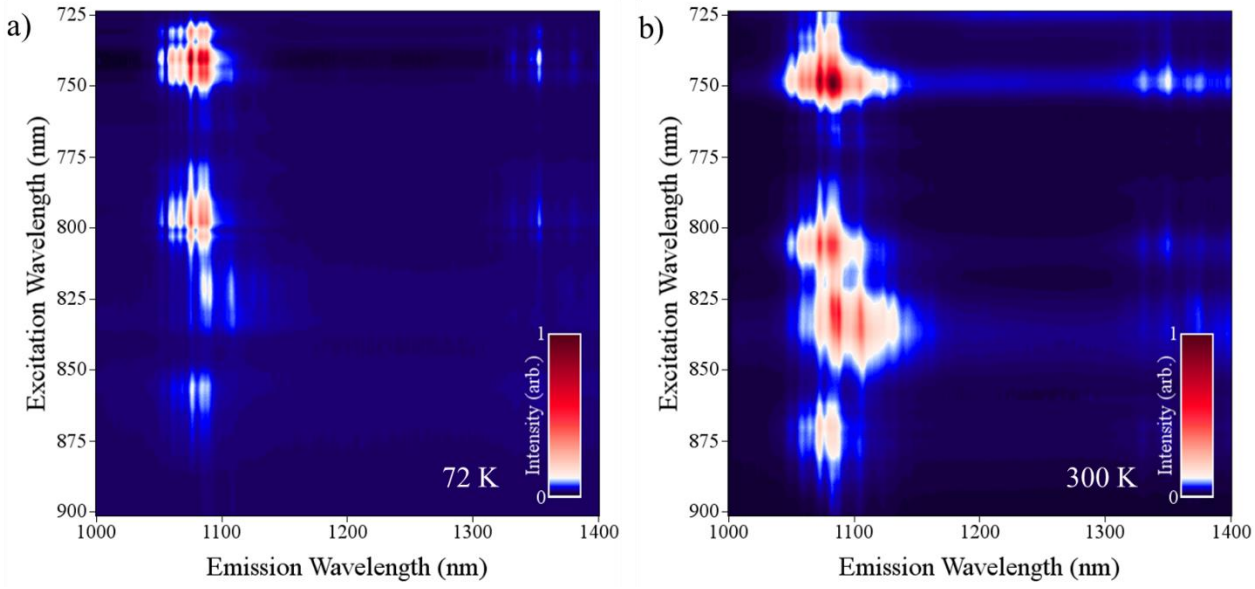

Figure 3. Luminescence vs. excitation maps for 0.5 at% Nd:AlN (Sample 2) taken with tunable laser pulse excitation at different temperatures. The intensities are normalized by the maximum (brightest) global emission peak. a) 300 K b) 72 K.

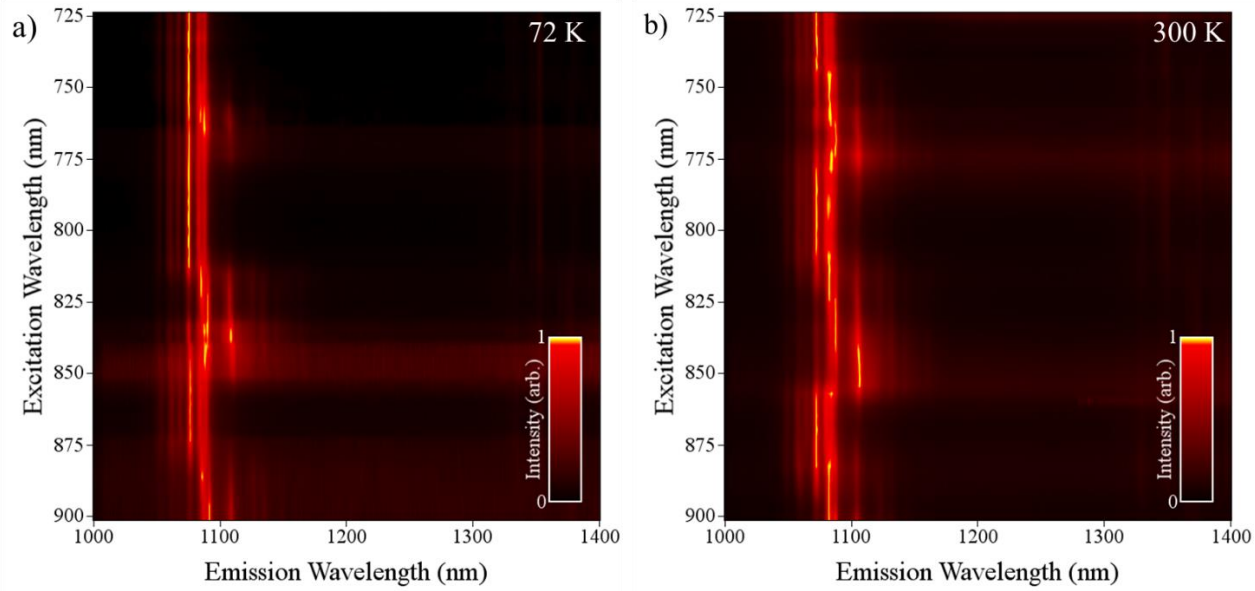

Figure 4. Luminescence vs. excitation maps for 0.5 Nd:AlN (Sample 2) taken with tunable laser pulse excitation at different temperatures. The intensities are normalized by maximum intensity for each excitation wavelength. a) 72 K and b) 300 K. Emission at 1077 nm dominates for nearly all excitation wavelengths except in the ~825-840 nm excitation range where ~1105 nm emission nearly rivals 1077 nm emission observed at other excitation wavelengths. This observation suggests the possibility for tuning based on pump wavelength.

b) **Nd:Alumina**

Like aluminum nitride, aluminum oxide has higher thermal conductivity than the state of the art (Nd:YAG).We have achieved remarkable success in this system; we have shown near theoretical transmission, emission with high brightness in Nd:Al203. See Figure 1.

Nitrides: We have been using lessons learned from Tb doping to establish processing conditions for Nd doping of AlN so that we can achieve emission in the IR. The results are promising so far, the samples are translucent. The optical quality will have to be improved in order to obtain lasing.

Our strategy for obtaining gain in Nd:Al_2O_3 is a twofold design of nano/microstructure that relies on: 1) Crystallite sizes below the wavelength of pump and emitted light 2) Dopant distribution in the grain volumes with minimal segregation at the grain boundaries. **Figure 5** summarizes our strategy. In ceramics with large grains, light is scattered at grain interfaces since they represent discontinuities in refractive index (**Fig. 5 a**), but the scattering efficiency of uniaxial grains is significantly lower in fine grains[26,27,30]. Thus fine grained ceramics can be highly transparent media with losses low enough to achieve optical gain (**Fig. 5 b**). In addition to low losses, RE dopant concentrations must be within a critical range; high enough to achieve a sufficient absorption cross section yet low enough to prevent concentration quenching (energy relaxation through phonon rather than radiative photon processes) which occurs when ions are too closely spaced. If the RE dopant solubility in the gain media is high, it is relatively easy to get a globally uniform RE distribution. However, in low solubility media, agglomeration occurs at grain boundaries (as shown in **Fig. 5a**). In the isotropic laser ceramics that have been demonstrated[11] grain sizes are typically 10-20 μm. In this case there is a relatively few grain boundaries regions and RE agglomeration quenches luminescence.

A key insight here is that the fine crystallite sizes that allow for high transparency can also play a crucial role in absorption/emission by providing a possibility for higher RE incorporation without luminescence

quenching. Grain boundary region increases as grain size decreases therefore holding the global concentration constant while decreasing grain size, RE dopants can 'spread out' along the grain boundaries increasing the average distance, $\tilde{l}$ between RE ions (**Fig. 5 b**). In other words, for *very fine grained materials, it should be possible to reach dopant concentrations sufficient to achieve gain even without solubility in the grain interior.* The effective grain size d_{eff} necessary to accommodate all of the dopants on the grain boundaries rather than grain interior depends on the arrangement of dopants on the boundary (function of $\tilde{l}$) and scales with $d^{3/2}$ (see Methods for details).

In order to illustrate this scenario, we plot d_{eff} as a function of grain size in **Fig. 5d** for various concentrations (at.% Nd) and dopant arrangements (**Fig. 5c)**. The shaded regions in **Fig. 5d** are conditions in which it is possible to accommodate the global concentration of dopant atoms, *c without any* solubility in the grain. In the non-shaded regions, $d_{eff} > d$ meaning that it is not possible to accommodate all of the dopant ions without solubility in the grain. In the limiting case example of a close packed monolayer ($\tilde{l} = 0$) (such as the one shown in **Fig 5c**) it is possible to accommodate c = 0.25 at.% of Nd on the grain boundary of a grain with d ~250 nm while for c = 0.5 at.% requires smaller grains, d = ~20 nm. The close packed monolayer case would not lead to gain since with ions this close together luminescence would surely be quenched. Using a realistic value of $\tilde{l}$ = 1 nm, we see that grain sizes < 25 nm are necessary to accommodate 0.25 at.% of Nd.

Fortunately, alumina does have Nd solubility which can be increased using high heating and cooling rates (to be discussed below), easing the necessity for extremely fine grains. The average grain sizes (AGS) of the ceramics produced in this work is ~250 nm and Nd:Al_2O_3 ceramics have minimal grain boundary segregation which result in materials with a high long range transparency (**Fig. 6a** and **b**) and that emit light at the characteristic Nd^{3+} wavelength of 1064 nm when pumped with 806 nm (**Fig. 6c**) which are prerequisites for gain.

We used a one-step, solid-state reaction densification approach for making transparent polycrystalline un-doped Al_2O_3 and Nd:Al_2O_3 ceramics by ***C***urrent ***A***ctivated ***P***ressure ***A***ssisted ***D***ensification (CAPAD). The CAPAD processing parameters were varied to optimize the microstructure and properties of various concentrations of Nd:Al_2O_3 (see methods for details). **Figure 6c** shows the effect of CAPAD temperature on the relative density of un-doped and samples doped with 0.25 and 0.35 at.% Nd (Nd:Al ratio). In all cases the heating rate was 300^{o}Cmin^{-1} and the temperature was held for 5 min. The results show a classic sigmoidal temperature dependence, where the density increases abruptly at a temperature referred to as the densification on-set temperature, T_{OD}. There is a clear influence of Nd dopant on T_{OD}. For the Nd doped Al_2O_3 samples, T_{OD} is ~200 ^{o}C higher that the un-doped case (a shift from ~900^{o}C to ~1100 ^{o}C). There is also a small effect between the two different Nd concentrations. The density of the 0.25 at.% Nd samples is slightly higher than the 0.35% at.% at most processing temperatures. Nd additions also affects the temperature required to obtain full density; Relative densities > 99% are achieved in the un-doped Al_2O_3 case at 1200 ^{o}C and ~ 1260 ^{o}C for the Nd:Al_2O_3 samples.

Reduced densification kinetics caused by RE additions in reaction/densification of ceramics has been reported before[13,31] and is due the homogenous presence of the RE oxide dopant powder primary along the particle/grain boundaries when the two phases are still separate reactants. In our previous work on alumina with Tb as a dopant, the decrease in density was lower compared to the presence of Nd at similar global concentrations[13].

The difference in behavior between the Nd and Tb dopants can be possibly attributed to the larger ionic radius of Nd^{3+} (0.983 Å) compared to Tb^{3+} (0.923 Å). A similar trend of a shift in the densification onset temperature with respect to RE ionic radius was reported for Nd^{3+}, Er^{3+}, and Eu^{3+} doped Al_2O_3 system (0.2 at.% RE:Al_2O_3 ratio) via free-sintering and hot-pressing by Drdlík *et al.*[32] It is worth noting that in their work, the densification T_{OD} was significantly higher than the present (>1400 ^{o}C) and a lower ~98% relative density was achieved at processing temperatures >1500 ^{o}C.

At processing temperatures of 1200 ^{o}C and 1260 ^{o}C the samples presented herein are transparent (to be discussed below). However, at 1300 ^{o}C all samples are opaque and white. This is due to an increased average grain size to ~2.1 µm ± 0.25 µm for the un-doped α-Al_2O_3, and 1.9 µm ± 0.22 µm and 1.87 µm ± 0.23µm, for the 0.25 at.% and 0.35 at.% Nd:Al_2O_3. At these larger grain sizes, the scattering efficiency is significantly higher (see **Fig. 5 a**).

Figure 6d shows X-Ray diffraction (XRD) profiles of the starting Al_2O_3 powder and polished Nd-doped ceramics produced using identical processing procedure (T=1260 ^{O}C, 5 min dwell, 105MPa). All samples (powders and densified ceramics) show only XRD peaks attributable to α-Al_2O_3 peaks *i.e.* no Nd_2O_3 dopant nor from ternary $NdAlO_3$ phase. This is in contrast to some previous reports that showed secondary phases in RE doped α-Al_2O_3[28,29] . Comparison of the powder and un-doped ceramic show no discernable difference. By contrast, the XRD spectra of the Nd doped samples reveal clear peak shifts to lower angles with increasing Nd concentration (Un-doped $2\theta = 35.18^{O}$, $2\theta_{0.25at.\%} = 34.09^{O}$ and $2\theta_{0.35at.\%} = 34.98^{O}$). The dashed line in the inset on the right is the location of highest intensity peak from literature. This shift is evidence of stretching of the α-Al_2O_3 lattice from the doping of Nd ions.

In order to further confirm incorporation of Nd into the alumina matrix, we performed transmission electron microscopy (TEM). A TEM micrograph as well as the corresponding Energy –dispersive X-ray Spectroscopy (EDS) distribution maps of a 0.35 at.% Nd:Al_2O_3 polycrystal (T = 1260 ^{O}C) are shown in **Figure 2e.** The brighter regions in the micrograph correspond to Nd rich areas. The EDS maps reveal that the Nd dopant is found in higher concentrations along some grain boundaries and triple points than within the grain interiors. Nonetheless, a significant portion of the Nd dopant is found within the matrix. It is interesting to discuss this level of dopant incorporation relative to Nd:YAG. The high Nd equilibrium solubility in YAG is due to the significantly more open crystal structure leading to a lower density compared to alumina (4.55 g/cm^3 for YAG, 3.99 g/cm^3 for α-Al_2O_3). Since Al_2O_3 is denser than YAG, the volume concentration, c_{vol} of Nd is significantly higher compared. At c = 0.25 at%, $c_{vol} = 1.18 \times 10^{20}$ for Nd:Al_2O_3 compared to $c_{vol} = 9.26 \times 10^{20}$ for Nd:YAG, an increase of ~26% .

We attribute the ability to accommodate concentrations as high as 0.35 at.% Nd (with minimal segregation) to the high heating and cooling rates we employed in processing. It is likely that the equilibrium solubility of Nd increases at higher temperatures so that fast cooling rate has the effect of "freezing in" Nd, while minimizing segregation. We employed cooling rates of ~ 300 ^{O}C.min^{-1} where cooling rates of 10-50 ^{o}C.min^{-1} are typical for traditional processing.

The high heating rate ~300^{o}C/min allow us to reach desired temperature quickly, minimizing unwanted grain growth[13,33]. We believe that the fine grain sizes of our ceramics (250 nm AGS) plays a crucial role in Nd incorporation as discussed (**Fig. 5**) Recent work by Rohrer, Harmer and coworkers on lanthanide doping of α-Al_2O_3 suggests that differences in grain boundary structure in un-doped *vs.* doped cases may play a role in the diffusion kinetics, and solubility of lanthanides[34,35], thus affecting the resultant microstructure. The concentration of grain boundaries increases with decreasing grain size and so if solubility of Nd is higher in the near-grain-boundary regions it is likely that fine grain sizes contribute to the incorporation of Nd dopants.

The high optical transparency of the consolidated bulk Nd:Al_2O_3 polycrystals can be qualitatively appreciated in the pictures in **Fig. 6** as discussed before. Pictures of both concentration of Nd:Al_2O_3 and un-doped Al_2O_3 are shown in **Fig. 7a** for comparison**.** The text is clearly legible below the ceramics, qualitatively showing high transparency. The high transparency corroborates the lack of second phases indicated by the XRD results since secondary phases would lead to significant scattering.

Transmission measurements of the Nd:Al_2O_3 and un-doped Al_2O_3 is shown in **Figure 7b**. In all cases, the transmission increases with wavelength and approaches the single crystal limit (losses due to Fresnel reflections only) at wavelengths greater than 1500 nm. The increase in transmission with wavelength can be explained by the decreasing efficiency of anisotropic scattering with wavelength as discussed before[26,27,30]. The transmission values of our un-doped alumina ceramics rival those previously reported for sinter-HIPed samples[26] and high pressure CAPAD.[36] More importantly, the Nd doped samples have similar transmissions. In the area of particular interest for lasing of typical Nd^{3+} media at ~1064 nm ($^4F_{3/2} \rightarrow {}^4I_{11/2}$ transition), the transmission is ~ 75% for the Nd:Al_2O_3. We attribute this high transmission to the high density (>99%) fine AGS (~ 250 nm), low Nd segregation and lack of undesired phases in the Nd:Al_2O_3.

One remarkable difference in the Nd doped *vs.* un-doped sample transmission spectra is the presence of the absorption bands centered at λ = 585 nm (2.12 eV), 748 nm (1.85 eV) and 806 nm (1.54 eV). These bands are in regions that have been consistently attributed to Stark transitions from the $^4I_{9/2}$ manifold in other Nd^{3+} gain media and is strong evidence of the presence of optically active Nd^{3+} within the doped ceramic matrix.[37] To the best of our knowledge this is the first time the presence of clear absorption bands associated with RE doping have been observed using a transmission measurement for polycrystalline Al_2O_3. Moreover, the depth of

the absorption bands increases with an increase in dopant concentration, indicating a higher degree of optical activity from the Nd^{3+} ion, in the 0.35 at.% sample.

Further confirmation of the presence of optically active Nd^{3+} within the α-Al_2O_3 matrix is observed in spontaneous photoluminescence (PL) resulting from optical pumping the absorption band at λ = 806 nm, causing emission at ~ 1060 nm from the $^4F_{3/2} \rightarrow {}^4I_{11/2}$ Nd^{3+} transition. **Figure 7c** presents the PL emission spectra for the 0.25 at.%, 0.35 at.% Nd^{3+}:Al_2O_3 samples as well as for 0.5 at.% Nd^{3+}:Glass (Schott), and 1.1 at.% Nd^{3+}:YAG (single crystal, Litton Technologies, Inc.), all pumped with the same laser diode used to obtain the infrared image in **Figure 6c.** Indeed, the Nd^{3+}:Al_2O_3 emit at similar wavelengths as the other laser quality hosts.

PL in RE:Al_2O_3 has been shown before. Krebs and Happek[28] used laser-heated pedestal growth (LHPG) to produce single-crystal Yb^{3+}:Al_2O_3 fibers and were able to determine that single-site doping of Yb^{3+} onto the Al^{3+} lattice was possible at concentrations below the RE solubility limit, but that at higher concentrations secondary phases that hindered PL formed. Sanamyan [29] *et al.* used CAPAD to form dense Er^{3+}:Al_2O_3 polycrystals with RE concentrations as high as 0.065% that showed PL. However, absorption or transmission measurements were not provided and it is likely that this dopant concentration is too low for gain. Together, the absorption, PL, XRD and TEM results in the present ceramics unambiguously show that Nd^{3+} existing at sufficient concentrations to absorb and emit light via direct diode pumping.

Comparison of Nd^{3+}:Al_2O_3 to Nd^{3+}:Glass an Nd^{3+}:YAG show emission in similar wavelengths but different line shapes. These commercially available laser media were chosen for comparison because the volumetric concentrations of Nd^{3+} ions are similar and because they are arguably the most important materials for high energy lasers. Nd^{3+}:Glass is the mainstay material for producing ultra-short, high peak power laser pulses from a Nd^{3+} [15,38] and Nd^{3+}:YAG is the most important gain media, including CW- and quasi CW-HEL-technology[9].

The single crystal profiles show narrow well defined peaks typical of single site doping. By contrast emission peaks in Nd^{3+}:Al_2O_3 appear heterogeneously broadened similar to Nd^{3+}:Glass although the overall PL bandwidth is wider than the laser glass. Heterogeneous broadening of the Nd^{3+}:Al_2O_3 emission lines is not surprising given that Nd ions are found on multiple sites including grain interiors, grain boundaries and triple points (**Fig. 6e**).

There are strong advantages to both sharp emission lines characteristic of single site doping as well as broadened lines (large emission bandwidth). Sharp emission lines usually lead to lower lasing thresholds while broadened lines can lead to amplification of shorter temporal pulses as well as pulses with very high energy.

In order to unambiguously ascertain the viability for lasing in Nd^{3+}:Al_2O_3 ceramics we measured their single pass gain. The schematic of the apparatus we used for measuring optical gain under direct diode pumping at λ = 806 nm (emission measured is λ = 1064 nm) is shown in **Figure 4a.** Briefly, the 1064 nm probe beam was passed through a specimen at a constant incident power and the transmitted intensity of the probe beam was monitored with a photodiode only sensitive to that wavelength. Simultaneously, in spatial counter-propagation, the specimen was pumped with an 806 nm laser diode by means of a dichroich optic. The increase/decrease in the probe beam intensity as a function of absorbed 806 nm pump power was monitored by the same photodiode. We used a modified version of the Beer-Lambert law for homogenous/Doppler broadened gain media to measure gain coefficients:

$$I(z) = I_o e^{[G]\cdot z} \qquad (2)$$

where I_o is the initial intensity of the probe beam, z is the sample thickness, and G is the gain coefficient. Negative gain in the presence of stimulated emission indicates that the losses of the media (combination of absorption, scattering, reflection, *etc.*) overcome the amplification of the incident stimulated emission resulting from external pumping. On the other hand, a positive G proves that the amplification of the stimulated emission probe beam surpasses the losses of the system, resulting in a net positive gain, *i.e.* amplification.

Figure 8b plots the results obtained from the single-pass pump/probe experiment for the 0.25 at.% and 0.35 at.% Nd^{3+}:Al_2O_3 ceramics as a function of absorbed pump power. Net positive gain is achieved at $P > 2.25$ W for both materials and the magnitude of G increases approximately linearly as a function of the absorbed pump power. As mentioned observation of gain is indicative of low losses (high optical quality) of the ceramics, and it proves the viability of lasing in Nd^{3+}:Al_2O_3. As the 806 nm pump power is increased the net positive gain

increases to values as high as 2.27 and 2.42 cm^{-1} for the 0.25 at.% and 0.35 at.% Nd^{3+} concentrations, respectively. G, is directly related to the product of the emission cross-section, σ, and the population difference of optically active photoelectrons in the excited state (N_E) and the ground state (N_G) such that[39]:

$$G = \sigma \cdot (N_E - N_G) \quad (3)$$

Since a negative σ is not possible in the presence of stimulated emission, a positive G, according Eq. 3 requires that $N_E > N_G$. Therefore, the measured positive gain coefficients also demonstrate population inversion in Nd:Al_2O_3 and prove the viability of Nd^{3+}:Al_2O_3 as a new laser gain media.

We attribute the successful demonstration of gain to the unique nanostructure of the ceramics. As discussed previously the ceramics have fine grain size and are Nd^{3+} doped. The incorporation into the grains and grain boundary regions is high enough to achieve significant luminescence without being overwhelmed by concentration quenching.

Given the demonstration of gain it is interesting to discuss the potential of Nd^{3+}:Al_2O_3 as a laser gain media. The gain bandwidth (G_{bw}) can be approximated from measuring the full-width at half-maximum (FWHM) of the normalized intensity of the PL spectra. From PL curves it is clear that the G_{bw} for Nd^{3+}:Al_2O_3 is significantly larger than for the commercial Nd^{3+} gain media **(Fig. 8X**). From FWHM of the Nd^{3+}:YAG Nd^{3+}:Glass we obtain G_{bw} = 0.6 nm (0.16 THz), for G_{bw} = 20 nm (5.4 THz), which agree well with previous measurements [37,38]. Remarkably the Nd^{3+}:Al_2O_3 G_{bw} = 49 nm (13 THz) and 48 nm (12.7 THz) for each dopant concentration. We believe these are the highest bandwidths measured for Nd^{3+} in a media with proven gain.

The importance of bandwidth is given by Fourier's theorem which dictates that the broader the emission bandwidth, the shorter the temporal pulses achievable by the gain media. The bandwidth-limited temporal pulse width, $\Delta\tau_P = 1/G_{bw}$. The large bandwidth of Nd^{3+}:Glass promises generation of high peak-power lasers by generation of ultra-short time pulses. Using G_{bw} measurements we find $\Delta\tau_P$ = 7.7 fs for 0.25 at.% Nd^{3+}:Al_2O_3, and $\Delta\tau_P$ = 7.9 fs for 0.35 at.% Nd^{3+}:Al_2O_3. These bandwidth-limited pulse widths represent a 2.5 fold increase in the single-shot peak power over Nd^{3+}:Glass and >80 fold increase over Nd^{3+}:YAG ($\Delta\tau_P$ = 6.3 ps for Nd^{3+}:YAG, $\Delta\tau_P$ =18.5 fs for Nd^{3+}:Glass).

In summary, we introduce an all solid-state powder processing route in conjunction with a single-step CAPAD reaction/densification to produce transparent bulk polycrystalline Nd^{3+}:Al_2O_3 with over-equilibrium Nd-doped (0.25 at.% and 0.35 at.%) concentrations. The ceramics have a transmission of ~75% at 1064 nm and display optical absorption bands at centered at λ = 585 nm, 748 nm and 806 nm, corresponding to the $^4G_{5/2}$, $^2H_{3/2}$, and $^4F_{9/2}$ Stark transitions from the $^4I_{9/2}$ manifold of optically active Nd^{3+}. We used single pass gain measurements to demonstrate gain and population inversion in a RE doped alumina ceramics for the first time. The estimated gain bandwidth, G_{bw}, for these materials is ~13 THz centered at 1064 nm and represents a new record for Nd^{3+} media with demonstrated gain. The resultant $\Delta\tau_P$, is very promising for short pulsed laser system as well as for producing high average power. Moreover, the significantly higher R_S ~19,500 W/m of Nd^{3+}:Al_2O_3 compared to R_S ~1 W/m Nd:Glass promise a significantly higher duty cycle, making Nd^{3+}:Al_2O_3 a truly game-changing gain material. Finally, we note that the nano/microstructural strategies demonstrated here should be applicable to many other oxide and nitride gain systems that were not previously believed to be applicable as laser ceramics and thus represents a fundamental shift in approach to producing new optical gain media.

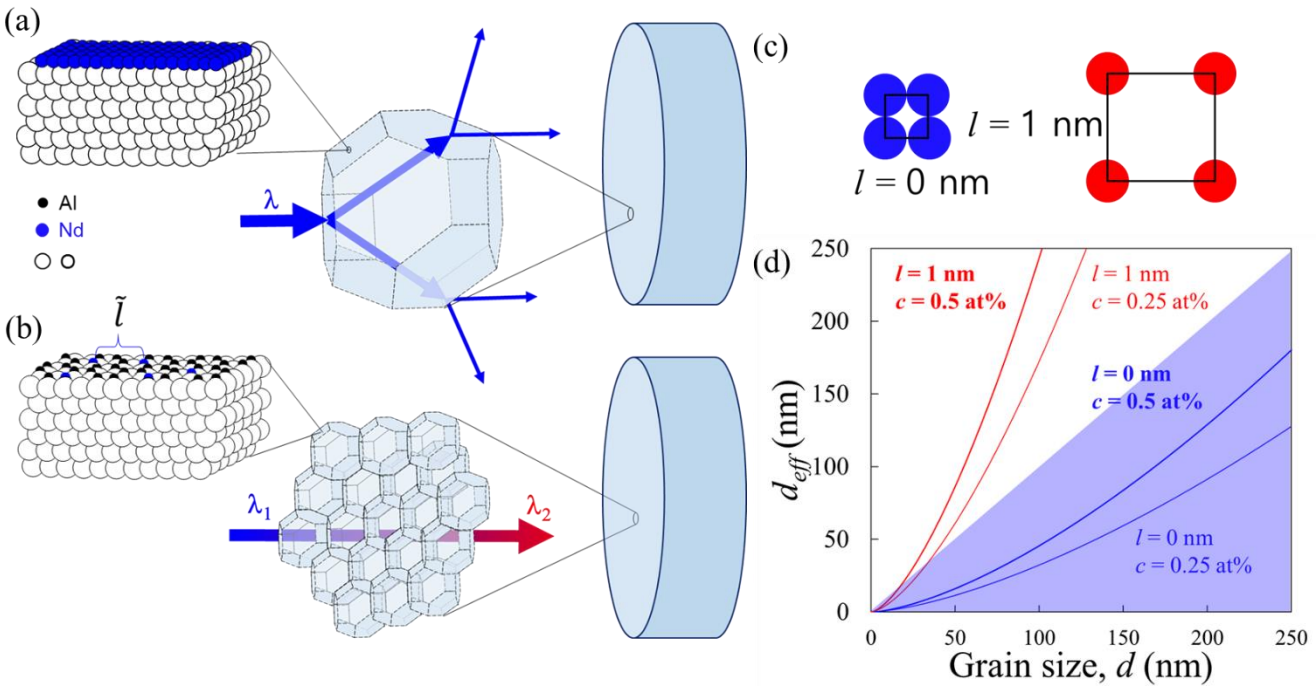

Figure 5. Length scale realtionships important for achieving gain (a) Light is scattered at grain interfaces in ceramics with large crystallites, since randomly oriented grains represent discontinuities in refractive index. RE segregation at grain boundary represented (close packed monolayer) on section ofAl2O3 (blue atoms are Nd, White are O and black are Al) (b) Scattering efficiency decreases significantly when pump (λ_1) and emitted light (λ_2) wavelengths are smaller than the grain size, permitting low optical losses. Small grains also permit spreading out of RE dopants at grain boundaries, increasing average interionic distance, $\tilde{l}$ allowing for optical gain. (c) A close packed arrangement of dopant l = 0 and one with realistic interionic distance for gain (l = 1 nm) (d) Calculation of grain size necessary to accommodate all of the dopants for given dopant arrangement and concentration on the grain boundary, d_{eff} *vs.* grain size using Eq. 4 for two concentrations and arrangements shown in (c).

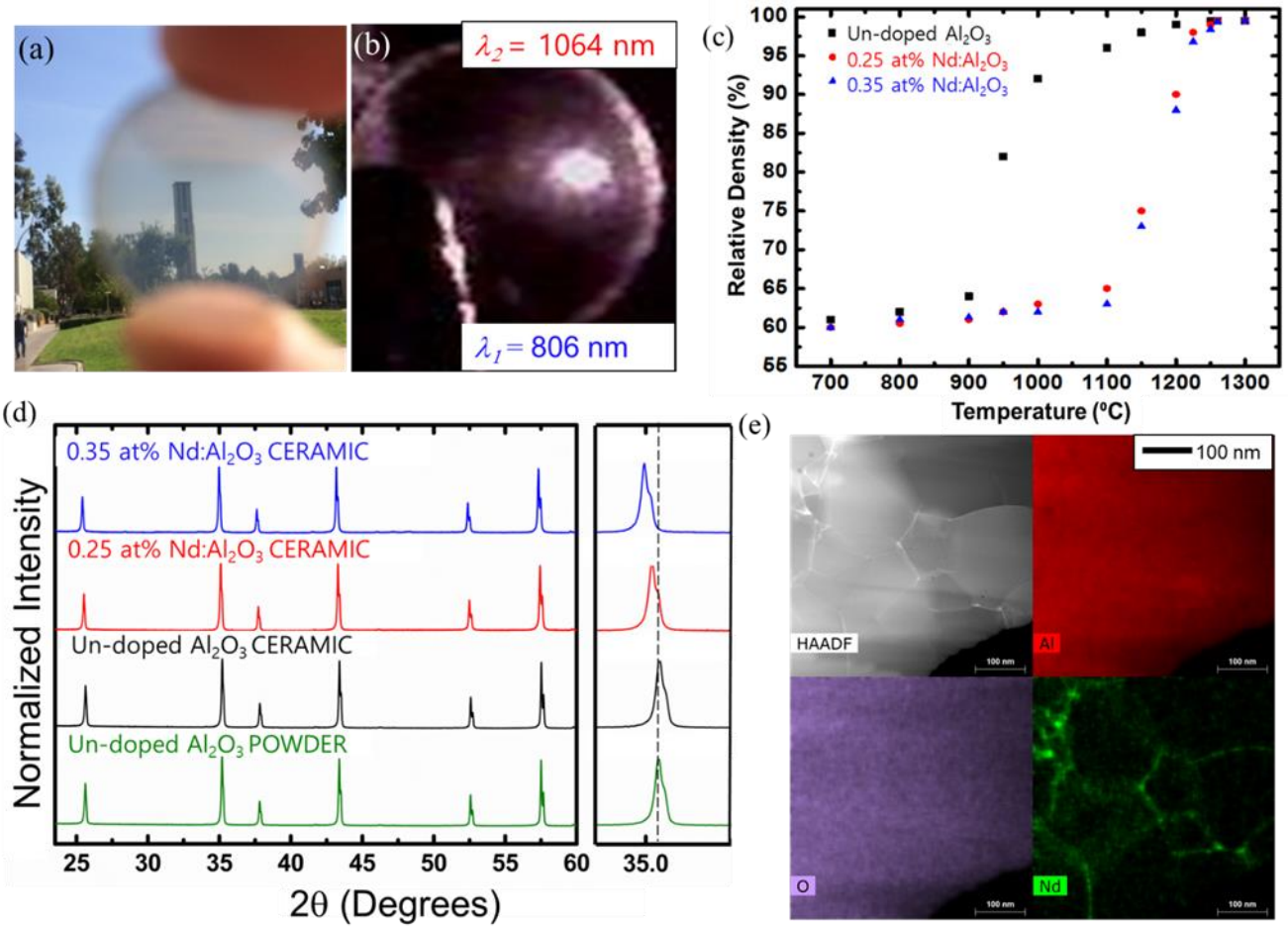

Figure 6. Physical and microstructural characterization of Nd: Al_2O_3. (a) Picture of, of clock tower viewed through 0.35 at% Nd:Al_2O_3 demonstrating high long range transparency. (b) Picture o fa 0.35 at% Nd:Al_2O_3 ceramic taken with a bandpass infrared camera (Transmission Band 1000 nm-1200 nm). The spot of light is the induced spontaneous PL in the near infrared from direct diode pumping at λ_1 = 806 nm. (c) the effect of CAPAD temperature on the relative density of un-doped and samples doped with 0.25 and 0.35 at.% Nd. (d) XRD profiles of the starting Al_2O_3 powder and Nd-doped ceramics. The inset on the right clearly shows peak shift relative to a α-Al_2O_3 standard (dashed line) for Nd:Al_2O_3 . (e) High-Angle Annular Dark-Field Transmission (HAADF) TEM micgrogarph of 0.35 at.% Nd:Al_2O_3 ceramic with corresponding EDS elemental maps for Al, O, and Nd (L-Lines). The EDS mapping reveals the presence of Nd along the grain boundaries and triple-points, but also within the grain interiors. The black portion of the maps along the bottom right hand corner pertains to a portion where no sample is present.

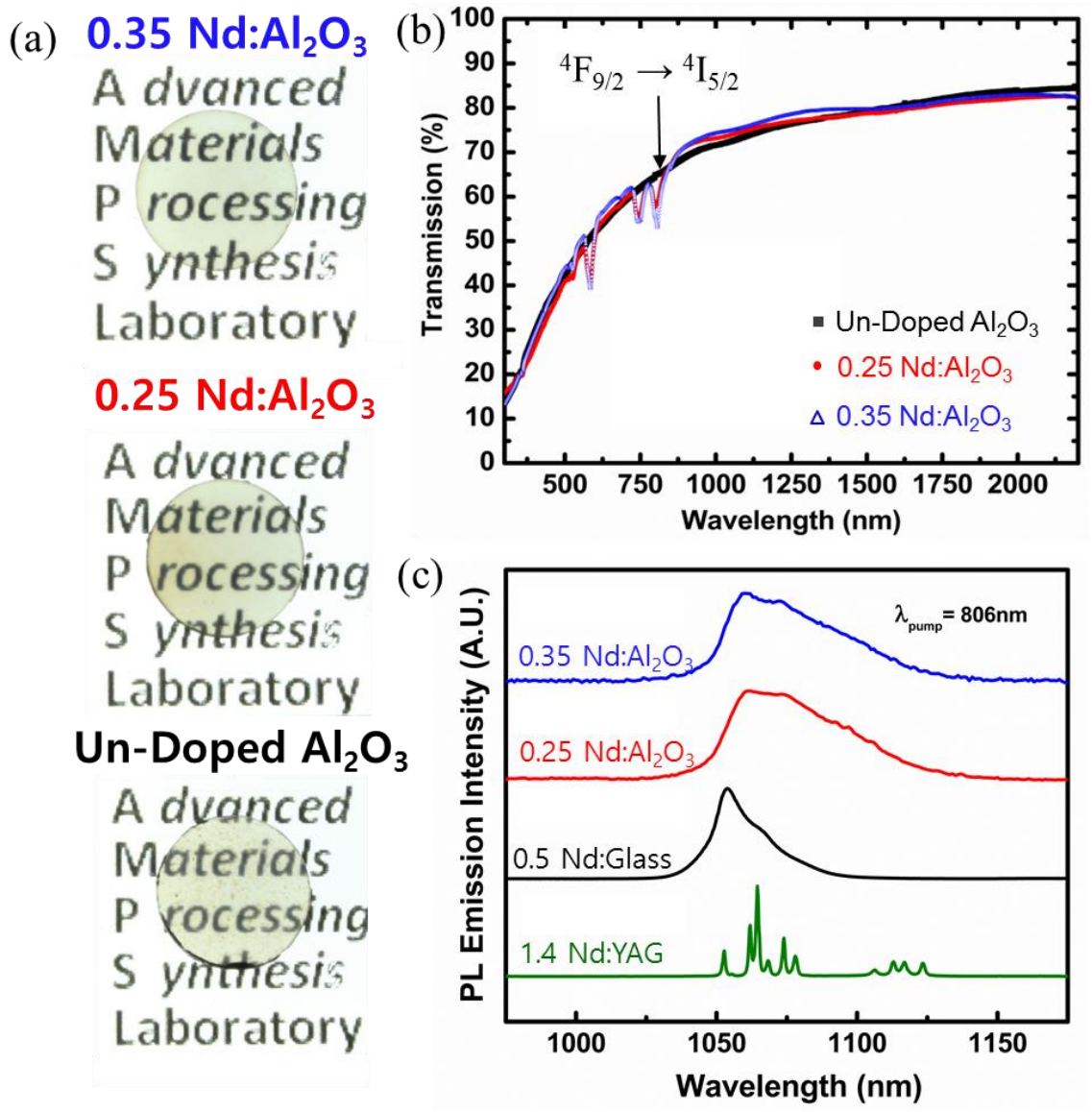

Figure 7. Optical Properties of of Nd: Al_2O_3. (a) Pictures of Nd-doped and un-doped ceramics. (b) Transmission measurements of the Nd:Al_2O_3 and un-doped Al_2O_3. All of the ceramics show high transmission and importantly the Nd-doped samples have absorption bands characteristic of Nd3+ transmission. The $^4F_{9/2} \rightarrow {}^4I_{5/2}$ band important for diode pumping is delineated with an arrow. (c) PL emission spectra for the 0.25 at.%, 0.35 at.% Nd^{3+}:Al_2O_3 samples along with 0.5 at.% Nd^{3+}:Glass, and 1.1 at.% Nd^{3+}:YAG single crystal. Pump source is an 806 nm laser diode. The PL reveal broadened lines attributed to the $^4F_{3/2} \rightarrow {}^4I_{11/2}$ electronic transitions.

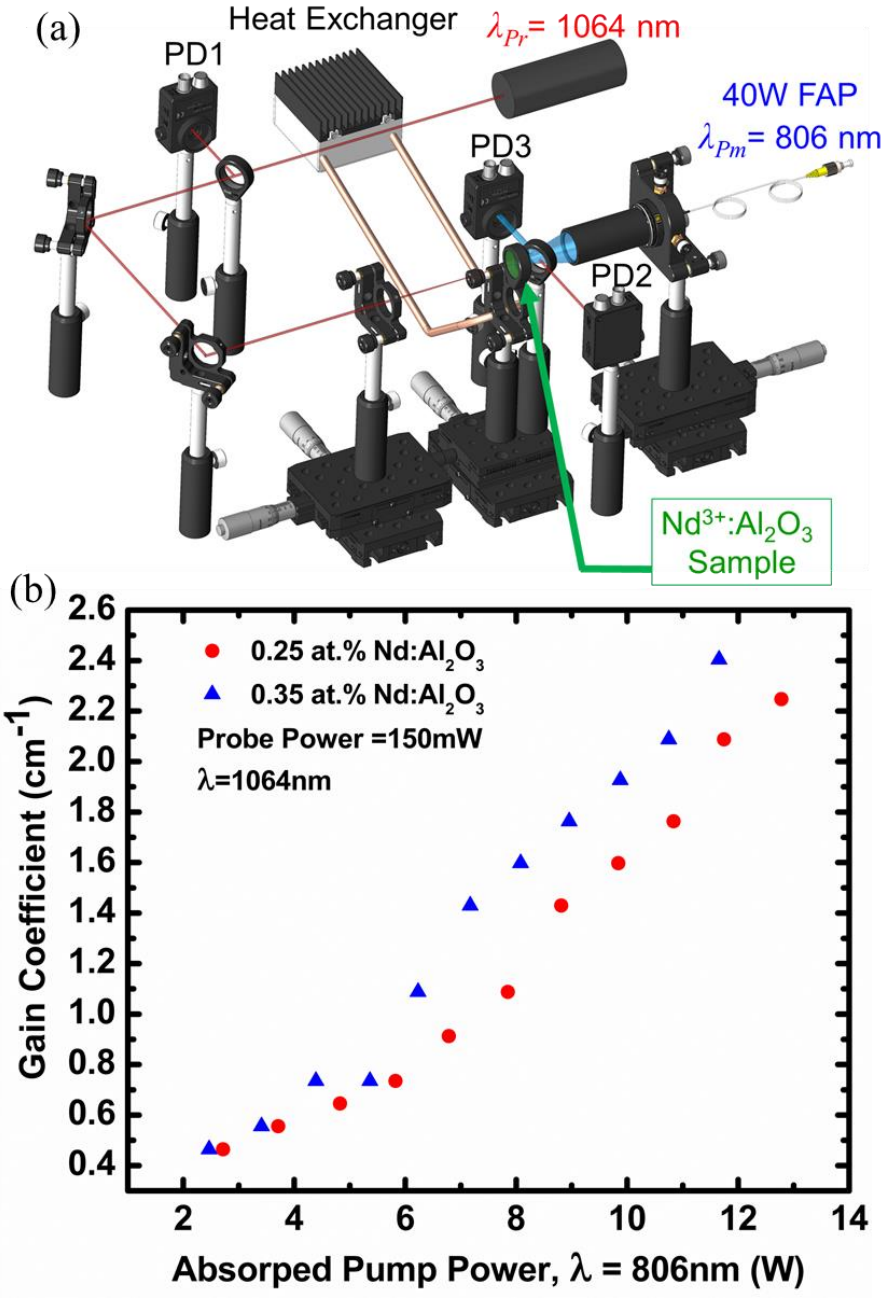

Figure 8 Demonstration of gain and population inversion **(a)** Schematic of the single-pass measurement set-up. (b) Single-pass gain coefficients of the 0.25 at.% and 0.35 at.% Nd^{3+}:Al_2O_3 bulk polycrystalline ceramics.

List of Publications

E. H. Penilla, Y. Kodera and J. E. Garay, “Blue-green emission in terbium doped alumina (Tb: Al_2O_3) transparent ceramics” *Advanced Functional Materials* (2013) **23**, 6036–6043

A. T. Wieg, Y. Kodera, Z. Wang, C. Dames and J. E. Garay
“Thermo-mechanical properties of rare earth doped AlN for laser applications: The role of grain boundaries and grain size” *Acta Materialia* (2015) **86**, 148-156.
V. Mishra, C. L. Hardin, J. E. Garay and C. Dames, "A 3 omega method to measure an arbitrary anisotropic thermal conductivity tensor", *Rev. of Sci. Instruments* **86** (2015) 054902

T. Hori, J. Shiomi, C. Dames, “Effective phonon mean free path in polycrystalline nanostructures.” *Applied Physics letters (*2015) **106**, 171901

A. T. Wieg, Y. Kodera, Z. Wang, C. Dames and J. E. Garay, “Thermomechanical properties of rare earth doped AlN for laser gain media: The role of grain boundaries and grain size” *Acta Materialia* (2015) **86**, 148-156.

E. H. Penilla, C. L. Hardin, Y. Kodera, S. A. Basun, D. R. Evans and J. E. Garay, “The role of scattering and absorption on the optical properties of birefringent polycrystalline ceramics: Modeling and experiments on ruby (Cr:Al_2O_3)” *Journal of Applied Physics* (2016) **119**, 023106

A. T. Wieg, M. J. Grossnickle, Y. Kodera, N. M. Gabor and J. E. Garay, “Nd:AlN polycrystalline ceramics: A candidate media for tunable, high energy, near IR lasers” *Applied Physics Letters* **109**, 121901 (2016)

A. T. Wieg, E. H. Penilla, C. R. Hardin, Y. Kodera and J. E. Garay, “Broadband white light emission from Ce:AlN ceramics: High thermal conductivity down-converters for LED and laser-driven solid state lighting” *APL Materials,* 4, 126105 (2016); doi: 10.1063/1.4971846 (2016)

E. H. Penilla, L. Devilla, M. Duarte C. Hardin, Y. Kodera, and J. E. Garay, “Gain in Nd doped alumina Transparent ceramics for high energy laser applications”, *Light: Science & Applications*. (2018) 7, doi:10.1038/s41377-018-0023-z

F. Kargar, E. H. Penilla, E. Aytan, J. S. Lewis, J. E. Garay and A. A. Balandin “Acoustic Phonon Spectrum Engineering in Bulk Crystals via Incorporation of Dopant Atoms” *Applied Physics Letters*. 112, 191902 (2018); doi: 10.1063/1.5030558

M. Duarte [a], V. Mishra [b], C. Dames [b], Y. Kodera [a] and J. E. Garay, “Processing and thermal conductivity of bulk nanocrystalline aluminum nitride.” *In review* (2019).

Students Graduated:
Andrew Weig PhD, 2015
Elias Penilla PhD 2016
Matthew Duarte PhD, Expected 2019